PNAS
www.pnas.org

Supplementary Information for

Intrinsic Spin of Elastic Waves

Yang Long, Jie Ren† and Hong Chen

†To whom correspondence should be addressed. E-mail: xonics@tongji.edu.cn

This PDF file includes:

Supporting Information Text

1. Intrinsic spin and energy flow

By using the tensor form, which is independent of the choice of coordinate system, the linear elastic wave equations can be written as(1):

$$\nabla \cdot \boldsymbol{\sigma} = \rho \frac{\partial^2 \boldsymbol{u}}{\partial t^2}, \tag{1}$$

where $\boldsymbol{\sigma} = \boldsymbol{C} : \boldsymbol{\varepsilon}$ is the Cauchy stress tensor, $\boldsymbol{\varepsilon} = \frac{1}{2}(\nabla \boldsymbol{u} + (\nabla \boldsymbol{u})^T)$ is the infinitesimal strain tensor, $\boldsymbol{u}$ is the displacement vector, $\boldsymbol{C}$ is the stiffness tensor, ρ is the mass density, the symbol : represents the inner product of two second-order tensors. We consider monochromatic elastic wave fields with frequency ω in a uniform non-dispersive solid, the linear elastic wave equations can be represented as $\nabla \cdot \boldsymbol{\sigma} = -\rho\omega^2 \boldsymbol{u}$ and the displacement field can be described by $\boldsymbol{u}(\boldsymbol{r}, t) = \boldsymbol{u}_0(\boldsymbol{r}) e^{-i\omega t}$.

The time-average Poynting vector density of elastic wave that describes the energy flux density is:

$$\boldsymbol{p} = -\frac{1}{2} Re[\boldsymbol{\sigma}^* \cdot \boldsymbol{v}], \tag{2}$$

where $\boldsymbol{v} = \frac{\partial}{\partial t}\boldsymbol{u} = -i\omega \boldsymbol{u}$ is the velocity of elastic wave and $Re[\cdot], Im[\cdot]$ mean operators to get real part and imaginary part. $\boldsymbol{v} = \frac{\partial \boldsymbol{u}}{\partial t} = -i\omega \boldsymbol{u}$, thus $\boldsymbol{p} = -\frac{\omega}{2} Im[\boldsymbol{\sigma}^* \cdot \boldsymbol{u}]$. In isotropic homogeneous solid, by using Lam*é* constants, one can get:

$$\boldsymbol{C} = \begin{pmatrix} 2\mu+\lambda & \lambda & \lambda & 0 & 0 & 0 \\ \lambda & 2\mu+\lambda & \lambda & 0 & 0 & 0 \\ \lambda & \lambda & 2\mu+\lambda & 0 & 0 & 0 \\ 0 & 0 & 0 & \mu & 0 & 0 \\ 0 & 0 & 0 & 0 & \mu & 0 \\ 0 & 0 & 0 & 0 & 0 & \mu \end{pmatrix}, \tag{3}$$

where $\lambda = K - \frac{2}{3}G$, $\mu = G$, K is the bulk modulus and G is the shear modulus.

As we know, the Poynting vector $\boldsymbol{p}$ describes the directional energy flux density of elastic wave. In fact it represents a sum of two terms with quite different physical meanings. Thus, one can write $\boldsymbol{p}$ into the form:

$$\boldsymbol{p} = \boldsymbol{p}^o + \boldsymbol{p}^s, \tag{4}$$

where $\boldsymbol{p}^o$ and $\boldsymbol{p}^s$ represent the orbital and spin constituents of the total energy flow(2). To unveil the intrinsic spin of elastic wave, we discuss it based on the longitudinal and transverse part separately. For longitudinal part $\boldsymbol{u}_L$, it satisfies the relation $\nabla \times \boldsymbol{u}_L = 0$, and the time-average Poynting density can be written as:

$$\begin{aligned} \boldsymbol{p}_L &= \frac{\omega}{2}\left((2\mu+\lambda)\mathrm{Im}[\boldsymbol{u}_L^* \cdot (\nabla)\boldsymbol{u}_L] + \frac{\lambda}{2}\nabla \times \mathrm{Im}[\boldsymbol{u}_L^* \times \boldsymbol{u}_L]\right) \\ &= \boldsymbol{p}_L^o + \boldsymbol{p}_L^s, \end{aligned} \tag{5}$$

where

$$\begin{aligned} \boldsymbol{p}_L^o &= \frac{\omega}{2}(2\mu+\lambda)\mathrm{Im}[\boldsymbol{u}_L^* \cdot (\nabla)\boldsymbol{u}_L] = \frac{\omega}{2}\rho v_L^2 \mathrm{Im}[\boldsymbol{u}_L^* \cdot (\nabla)\boldsymbol{u}_L] \\ \boldsymbol{p}_L^s &= \frac{\omega}{2}\frac{\lambda}{2}\nabla \times \mathrm{Im}[\boldsymbol{u}_L^* \times \boldsymbol{u}_L], \end{aligned} \tag{6}$$

with v_L the velocity and $\boldsymbol{u}_L$ the displacement field of longitudinal wave. Here, $\boldsymbol{p}_L^o$, the canonical or orbital Poynting density, is responsible for the energy transport of elastic longitudinal wave. $\boldsymbol{p}_L^s$, the spin Poynting density, does not transport energy but is originated from the spin angular momentum of elastic longitudinal wave.

For transverse part $\boldsymbol{u}_T$, it satisfies the relation $\nabla \cdot \boldsymbol{u}_T = 0$, and the time-average Poynting density can be written as:

$$\begin{aligned} \boldsymbol{p}_T &= \frac{\omega}{2}\left(\mu\mathrm{Im}[\boldsymbol{u}_T^* \cdot (\nabla)\boldsymbol{u}_T] + \frac{\mu}{2}\nabla \times \mathrm{Im}[\boldsymbol{u}_T^* \times \boldsymbol{u}_T]\right) \\ &= \boldsymbol{p}_T^o + \boldsymbol{p}_T^s, \end{aligned} \tag{7}$$

where

$$\begin{aligned} \boldsymbol{p}_T^o &= \frac{\omega}{2}\mu\mathrm{Im}[\boldsymbol{u}_T^* \cdot (\nabla)\boldsymbol{u}_T] = \frac{\omega}{2}\rho v_T^2 \mathrm{Im}[\boldsymbol{u}_T^* \cdot (\nabla)\boldsymbol{u}_T] \\ \boldsymbol{p}_T^s &= \frac{\omega}{2}\frac{\mu}{2}\nabla \times \mathrm{Im}[\boldsymbol{u}_T^* \times \boldsymbol{u}_T]. \end{aligned} \tag{8}$$

v_T is the speed of transverse wave. $\boldsymbol{p}_T^o$ and $\boldsymbol{p}_T^s$ have similar physical meanings like their longitudinal wave counterparts.

For the complicated elastic wave with both longitudinal and transverse components, the total displacement field is $\boldsymbol{u} = \boldsymbol{u}_L + \boldsymbol{u}_T$, but the Poynting vector $\boldsymbol{p}$ can not be represented by the linear sum of orbital and spin Poynting vectors of transverse part and longitudinal part, which means $\boldsymbol{p} \neq \boldsymbol{p}_L^o + \boldsymbol{p}_L^s + \boldsymbol{p}_T^o + \boldsymbol{p}_T^s$. By analyzing the physics described by the mathematical definition, the total Poynting density $\boldsymbol{p}$ can be dissected into a sum of terms with quite different physical meanings:

$$\boldsymbol{p} = \boldsymbol{p}_L^o + \boldsymbol{p}_L^s + \boldsymbol{p}_T^o + \boldsymbol{p}_T^s + \boldsymbol{p}_h^o + \boldsymbol{p}_h^s, \tag{9}$$

where $\boldsymbol{p}_h^o = \frac{\omega}{2}\rho v_L^2 \mathrm{Im}[\boldsymbol{u}_T^* \cdot (\nabla)\boldsymbol{u}_L] + \frac{\omega}{2}\rho v_T^2 \mathrm{Im}[\boldsymbol{u}_L^* \cdot (\nabla)\boldsymbol{u}_T]$ is the hybrid orbital Poynting density when transverse and longitudinal propagating waves with non-parallel directions meet in solid and $\boldsymbol{p}_h^s = \frac{\omega}{2}\frac{\lambda+2\mu}{2}\nabla \times \mathrm{Im}[\boldsymbol{u}_T^* \times \boldsymbol{u}_L + \boldsymbol{u}_L^* \times \boldsymbol{u}_T]$ is the extra energy flux raised from hybrid spin in mixed longitudinal-transverse wave.

Using the state vector introduced in main text, the orbital and spin Poynting vector can be written as 'local expectation values' of the corresponding operators:

$$\begin{aligned}
\boldsymbol{p}_L^o &= \mathrm{Re}[\langle \boldsymbol{u}_L | \hat{\boldsymbol{p}}_L | \boldsymbol{u}_L \rangle] \\
\boldsymbol{p}_T^o &= \mathrm{Re}[\langle \boldsymbol{u}_T | \hat{\boldsymbol{p}}_T | \boldsymbol{u}_T \rangle] \\
\boldsymbol{p}_h^o &= \mathrm{Re}[\langle \boldsymbol{u}_T | \hat{\boldsymbol{p}}_L | \psi_L \rangle + \langle \boldsymbol{u}_L | \hat{\boldsymbol{p}}_T | \boldsymbol{u}_T \rangle] \\
\boldsymbol{p}_L^s &\propto \nabla \times \langle \boldsymbol{u}_L | \hat{\boldsymbol{S}} | \boldsymbol{u}_L \rangle \\
\boldsymbol{p}_T^s &\propto \nabla \times \langle \boldsymbol{u}_T | \hat{\boldsymbol{S}} | \boldsymbol{u}_T \rangle \\
\boldsymbol{p}_h^s &\propto \nabla \times (\langle \boldsymbol{u}_T | \hat{\boldsymbol{S}} | \boldsymbol{u}_T \rangle + \langle \boldsymbol{u}_L | \hat{\boldsymbol{S}} | \boldsymbol{u}_T \rangle)
\end{aligned} \tag{10}$$

where $\hat{\boldsymbol{p}}_{L,T} = -iv_{L,T}^2\nabla$ are the orbital Poynting density operators and $\hat{\boldsymbol{S}}$ is the spin-1 angular momentum density operator for elastic wave, with $\boldsymbol{u}^* \cdot (\hat{\boldsymbol{S}})\boldsymbol{u} = \mathrm{Im}[\boldsymbol{u}^* \times \boldsymbol{u}]$ (3–6). From the results, we can find that the spin of elastic wave plays an important role in energy transport and specially, the hybrid spin can induce non-trivial contribution for Poynting vector in mixed transverse-longitudinal wave.

Beside the spin texture cases in the main text, there is another intriguing spin distribution: two dimensional spin lattice. To induce 2D spin lattice, it is simple to achieve so by exploiting the linear superposition of two longitudinal-transverse mixed elastic waves: $\boldsymbol{u} = \boldsymbol{u}_1 + \boldsymbol{u}_2$, as shown in Fig. S1:

$$\begin{aligned}
\boldsymbol{u}_{1/2} &= \boldsymbol{u}_{L,1/2} + \boldsymbol{u}_{T,1/2} \\
\boldsymbol{u}_{L,1} &\propto \exp(ik_L y)\boldsymbol{e}_y \\
\boldsymbol{u}_{L,2} &\propto \exp(ik_L x)\boldsymbol{e}_x \\
\boldsymbol{u}_{T,1} &\propto \exp(ik_T y)\boldsymbol{e}_x \\
\boldsymbol{u}_{T,2} &\propto \exp(ik_T x)\boldsymbol{e}_y
\end{aligned} \tag{11}$$

The corresponding quantum elastic spin can be derived as the following forms:

$$\begin{aligned}
\boldsymbol{s} &= \boldsymbol{s}_L + \boldsymbol{s}_T + \boldsymbol{s}_h \\
\boldsymbol{s}_L &\propto -2\sin(k_L(x-y))\boldsymbol{e}_z \\
\boldsymbol{s}_T &\propto 2\sin(k_T(x-y))\boldsymbol{e}_z \\
\boldsymbol{s}_h &\propto (\sin((k_L - k_T)y) - \sin((k_L - k_T)x))\boldsymbol{e}_z
\end{aligned} \tag{12}$$

where $k_{L,T}$ are the wave vectors of longitudinal and transverse wave. The total spin $\boldsymbol{s}$ will vary periodically in two dimensions shown in Fig. S1. Non-zero spatial partial differential of $\boldsymbol{s}_h$ will induce non-trivial observable energy flow distribution $\boldsymbol{p}_h^s \propto \nabla \times \boldsymbol{s}_h \neq 0$.

2. Non-trivial Spin in spatial confined wave fields

In isotropic homogeneous solid, for the displacement field of elastic wave propagating along z direction, as shown in Fig. S2(a), it only carries the orbital Poynting vector: $\boldsymbol{p}^o \propto |\boldsymbol{p}^o|\boldsymbol{e}_z$, while the spin Poynting vector vanishes: $\boldsymbol{p}^s = \boldsymbol{0}$ because the spin currents from the neighbouring loops cancel with each other (4). The plane wave solution is an unbounded state for elastic wave, but for the evanescent cases with boundary or spatially confined elastic waves, there will immediately induce a non-zero spin current shown in Fig. S2(b), namely, $\boldsymbol{p}^s \neq 0$, which can yield non-zero spin $\boldsymbol{s}$. Thus, the physical mechanism dependent on the spin can not be observed in bulk isotropic homogeneous solid due to the degenerated (cancelled) spin states, but it will be valid on the evanescent waves or spatially confined cases (like Gaussian decay case), which can hold non-zero spin and support the spin-dependent states.

Consider a single evanescent wave propagating along the x axis and decaying in the $y > 0$ half-space, namely, $\boldsymbol{u}_E \propto \exp(ikx)\exp(-i\omega t)$, one can decompose the wave into longitudinal and transverse parts in isotropic homogeneous solid: $\boldsymbol{u}_E = \boldsymbol{u}_{L,E} + \boldsymbol{u}_{T,E}$, $|\boldsymbol{u}_{L,E}| \propto \exp(-\kappa_L y)$, $|\boldsymbol{u}_{T,E}| \propto \exp(-\kappa_T y)$. According to the conditions $\nabla \times \boldsymbol{u}_{L,E} = 0$ and $\nabla \cdot \boldsymbol{u}_{T,E} = 0$, we obtain the evanescent wave forms:

$$\begin{aligned}
\boldsymbol{u}_{L,E} &= u_{0,L}\begin{pmatrix} 1 \\ i\frac{\kappa_L}{k} \\ 0 \end{pmatrix}\exp(ikx - \kappa_L y), \\
\boldsymbol{u}_{T,E} &= u_{0,T}\begin{pmatrix} -i\frac{\kappa_T}{k} \\ 1 \\ 0 \end{pmatrix}\exp(ikx - \kappa_T y),
\end{aligned} \tag{13}$$

where $k^2 - \kappa_{L,T}^2 = \frac{\omega^2}{v_{L,T}^2}$.

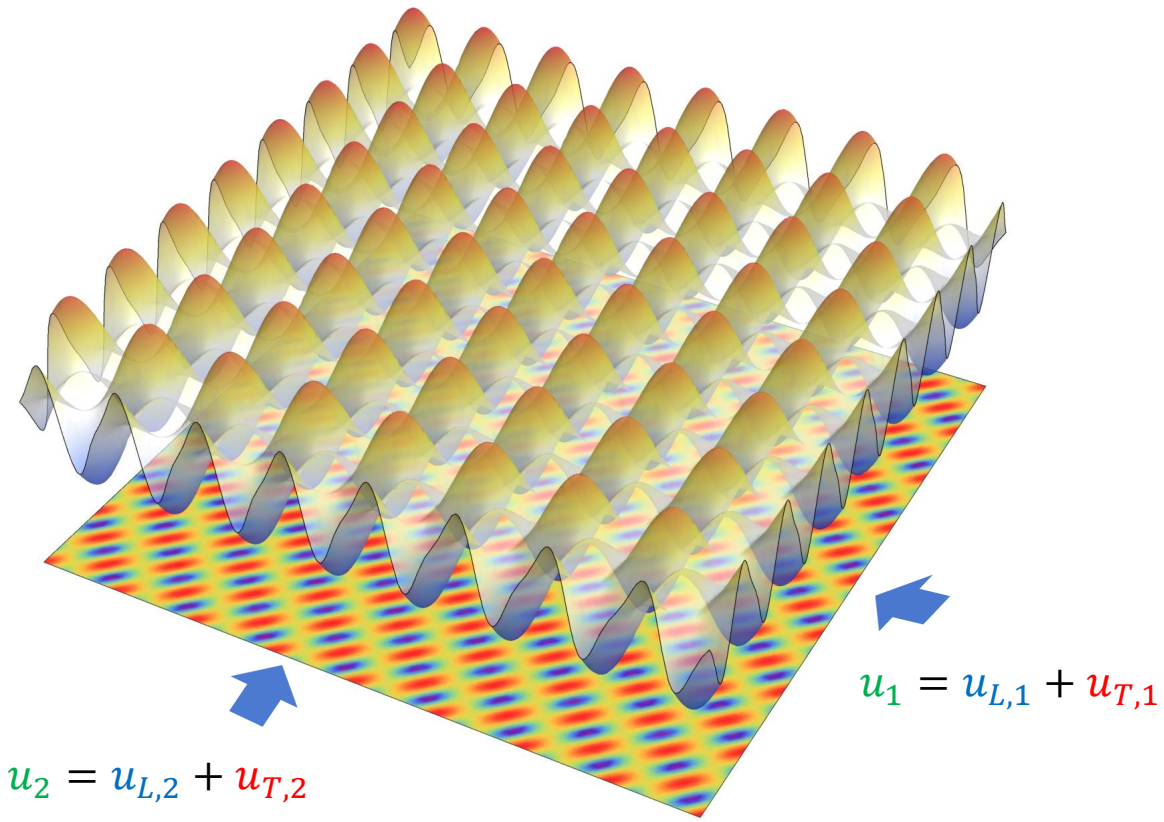

Fig. S1. Two dimensional spin lattice. The hybrid spin angular density(top plane, the color from red to blue denotes the spin value from maximal to minimal) of the total elastic waves (bottom plane, the color from red to blue denotes the displacement value from maximal to minimal) will behave in two-dimensional lattice form.

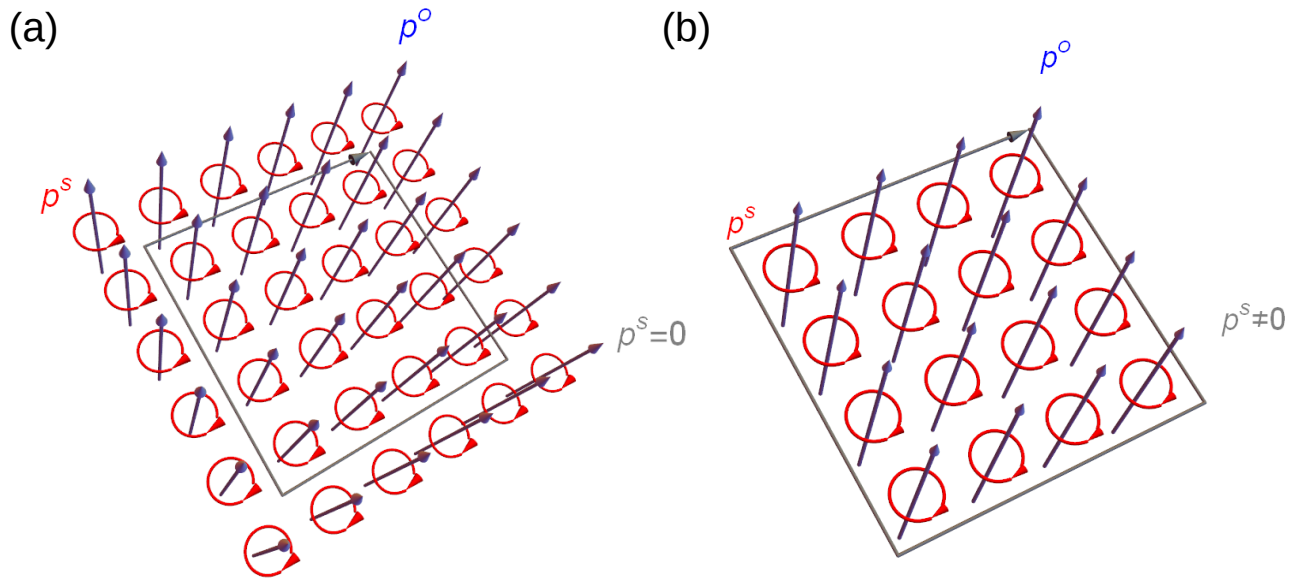

Fig. S2. For elastic wave in unbound isotropic solid (a), the spin currents from neighboring loop cancel with each other, which make the spin Poynting vector $\boldsymbol{p}^s$ vanishes, $\boldsymbol{p}^s = \mathbf{0}$. But for bound media or spatially confined elastic wave in isotropic materials (b), the case will be different. Non-zero circulation of spin currents will induce non-zero spin current, namely, $\boldsymbol{p}^s \neq 0$.

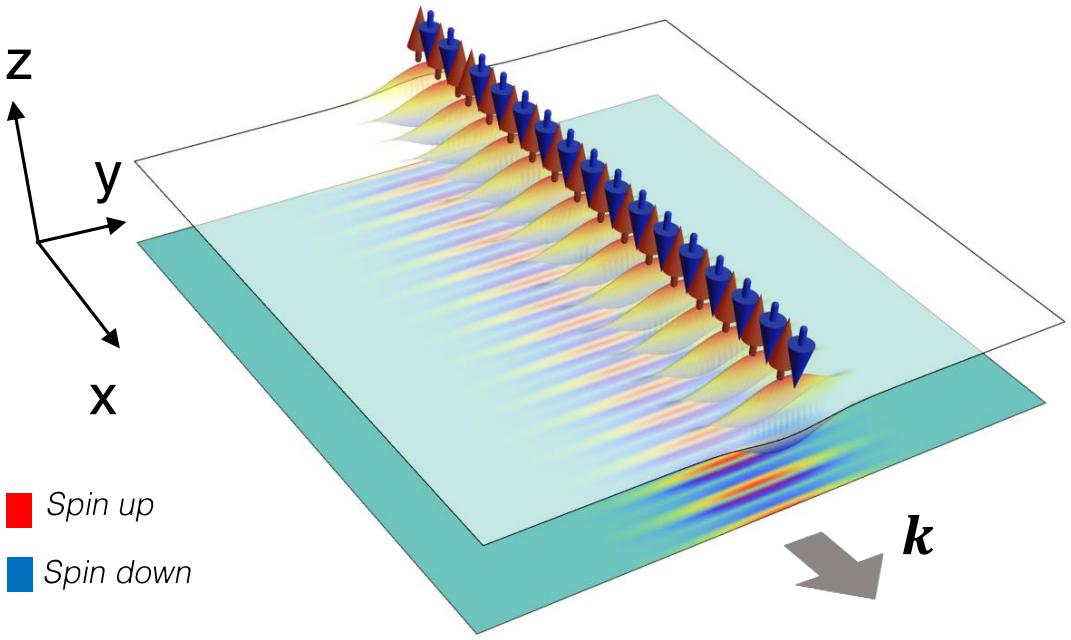

Fig. S3. Spin texture in mixed longitudinal-transverse elastic wave of Gaussian beam. The hybrid spin density of mixed longitudinal-transverse wave Gaussian beam is plotted.

By using the spin angular momentum operators, we can calculate their corresponding spin density values in the evanescent wave:

$$\begin{aligned} \boldsymbol{s}_L &\propto \frac{2\kappa_L}{k}\exp(-2\kappa_L y)\boldsymbol{e}_z, \\ \boldsymbol{s}_T &\propto \frac{2\kappa_T}{k}\exp(-2\kappa_T y)\boldsymbol{e}_z. \end{aligned} \quad [14]$$

The physical mechanism behind the generation of non-zero spin densities is that the inhomogeneous energy intensity (namely, the displacement field strength), which can destroy the cancellation of the spin current loops in bulk propagation wave. The total spin of elastic wave $\boldsymbol{u}_E$ will be $\boldsymbol{s} = \boldsymbol{s}_L + \boldsymbol{s}_T$, the hybrid spin $\boldsymbol{s}_h$ vanishes due to the cancellation of spin projection, $\langle \boldsymbol{u}_{L,E}|\hat{\boldsymbol{S}}|\boldsymbol{u}_{T,E}\rangle + \langle \boldsymbol{u}_{T,E}|\hat{\boldsymbol{S}}|\boldsymbol{u}_{L,E}\rangle = 0$.

In the main text, we show that the Gaussian beam of elastic longitudinal wave can hold non-trivial spin density. For the Gaussian longitudinal wave form in xOy plane, $|\boldsymbol{u}| \propto \exp(-y^2/\delta^2)$, we can find the non-trivial spin density. Considering the longitudinal wave Gaussian beam in high frequency and the width δ is larger than wave length, $\delta \gg \lambda_L$, one can ignore the beam divergence, $k \approx k_L$. Thus the longitudinal Gaussian wave beam can be written as:

$$\boldsymbol{u}_{L,G} = u_0 \begin{pmatrix} 1 \\ \frac{2iy}{k_L\delta^2} \\ 0 \end{pmatrix} \exp(-\frac{y^2}{\delta^2})\exp(ik_L x - \omega t). \quad [15]$$

One can calculate its corresponding spin density by using the spin angular momentum operator:

$$\boldsymbol{s} \propto \frac{4y}{k_L\delta^2}\exp(-\frac{2y^2}{\delta^2})\boldsymbol{e}_z. \quad [16]$$

Different with the evanescent wave at single-side boundary, the Gaussian wave beam can hold two opposite spin distribution simultaneously on both sides of beam: $s_z > 0$ for $y > 0$, and $s_z < 0$ for $y < 0$. As discussed in the main text, this spin texture in Gaussian beam is locked with momentum $\boldsymbol{k}_L$, which can reflect its intrinsic geometric properties.

We also calculate the hybrid spin density of the elastic field that contains both longitudinal and transverse Gaussian beams simultaneously, as shown in Fig. S3. In this case, the hybrid spin from longitudinal-transverse mixing concentrates mainly on the center area and has a periodic flipping form along x.

3. Spin momentum locking: Quantum spin Hall effect

Spin-momentum locking of surface mode is one main feature in quantum spin Hall effect (QSHE) (7, 8) and 3D topological insulators (9, 10), which defines the strong locking relation between spin profile and momentum direction. Here, we will show that non-trivial strong spin-momentum locking of elastic wave exists at the boundary of solid. It is well known that there exists one kind of surface wave $\boldsymbol{u}_{surf}$ on solid, Rayleigh wave, which is combination of longitudinal and transverse waves and has the evanescent wave form normal to solid surface. The spin angular momentum density $\boldsymbol{s}_{surf}$ of Rayleigh wave shown in Fig. S4(a)

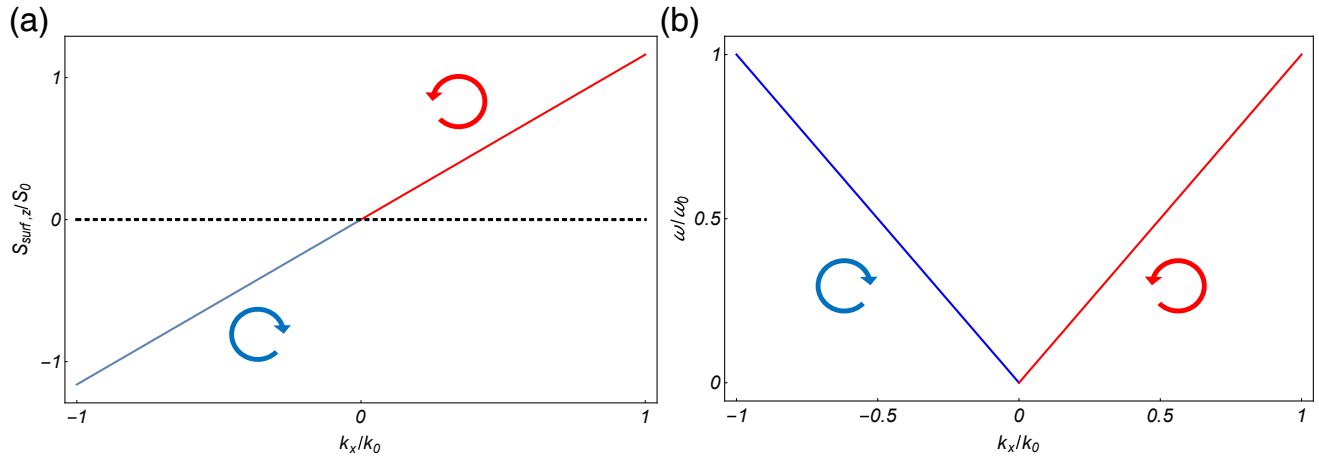

Fig. S4. Strong spin-momentum locking phenomena on elastic surface mode.(a) Spin densities of Rayleigh wave vs momentum, which shows that spin-momentum locking. (b) Dispersion relationship of Rayleigh wave on aluminum surface, the color represent the sign of their corresponding spin densities: Red: $\boldsymbol{s}_{surf,z} > 0$ and Blue: $\boldsymbol{s}_{surf,z} < 0$.

reveal strong spin-momentum locking, similar to that in QSHE (7, 8) and 3D topological insulators for electrons (11, 12): The Rayleigh wave with $k > 0$ and $k < 0$ will have opposite spin angular momentum densities $s_{surf,z} > 0$ and $s_{surf,z} < 0$ shown in Fig. S4(b). Thus, similar with light, the surface mode of solid, Rayleigh wave with evanescent form exhibits counter propagating opposite-spin edge modes, i.e., the QSHE of elastic wave.

A. Not robust surface elastic wave . Here, we will discuss the robustness of the surface elastic mode. As we know, one of the basic models of 3D topological insulators is based on the Dirac equation for a relativistic electron (13, 14). A planar interface between two half-spaces, where electrons are described by the Dirac equations with positive and negative masses, supports topological surface states. These modes are known as Jackiw-Rebbi surface modes (13, 14). And their forward- and backward-propagating waves have orthogonal polarization spinors, which can be related to the fact that the topological Jackiw-Rebbi modes represent helical massless fermions and they have suppressed backscattering and are robust against disorder (11, 12). As discussed above, the surface elastic wave modes, Rayleigh wave, can have the main feature of QSHE: spin-momentum locking. However, unlike the topological Jackiw-Rebbi modes, the surface elastic wave modes, similar to the QSHE of light (3), have a fixed spinor that is independent of the momentum. This is related to the fact that the surface elastic wave modes are not helical fermion, but have usual scattering properties and are not robust against impurities or disorder. Thus, one can say that surface elastic modes exhibit unidirectional spin-related transport (QSHE) but with trivial $\mathbb{Z}_2$ topological properties ($\frac{C_{spin}}{2} \mod 2 = 0$, $C_{spin} = C^L_{spin} + C^T_{spin} = 4$).

B. Spin-selected elastic wave routing. Non-trivial spin-momentum locking have shown to occur on the surface (boundary) of an isotropic solid. The similar spin-controlled excitation behavior can be also observed in anisotropic materials, interfacing with isotropic materials (15). Different from isotropic homogeneous solid, anisotropic materials may hold longer wave vectors compared with isotropic materials. When the beam in anisotropic media with large wave vectors meets the interface (set as $y = 0$) separating isotropic media and anisotropic media, it will induce total reflection and induce evanescent wave in isotropic media side ($y < 0$). This evanescent form of surface wave results in the circularly polarized profile: $\boldsymbol{u} = u_{L,0}(k/\tau_L, -i, 0)e^{ikx+\tau_L y} + u_{T,0}(ik/\tau_T, 1, 0)e^{ikx+\tau_T y}$. For this profile in the isotropic medium side, it will have the non-trivial spin density as:

$$\boldsymbol{s} = \langle \boldsymbol{u}|\hat{\boldsymbol{S}}|\boldsymbol{u}\rangle \propto -k\left(\frac{|u_{L,0}|^2}{\tau_L} + \frac{|u_{T,0}|^2}{\tau_T}\right), \qquad [17]$$

where $\tau_{L,T} = \sqrt{k^2 - k^2_{L,T}}$, and $k_{L,T} = \frac{\omega}{v_{L,T}}$. The key requirement on the spin-controlled elastic routing is the hyperbolic-like dispersion shown in Fig. S5(a), which is similar with the necessary condition for directional excitation of modes in hyperbolic optical metamaterials (15).

We note that although the selective elastic wave routing is in the anisotropic medium side, the chiral excitation of elastic spin is characterized in the isotropic medium side. Different spin excitation in the isotropic side selectively couples with the different directional wave routing in the anisotropic side through the selective evanescent waves of different spins at the interface. For the critical angles in hyperbolic dispersion, their densities of states (DOS) will become infinite, which implies that the emitted wave will propagate within the extraordinary modes forming a cone with an opening critical angles. And meanwhile, these high DOS modes in a hyperbolic metamaterial would be made up of the superposition of different components with $k > k_{L,T}$ or $k < -k_{L,T}$, which induces evanescent waves in isotropic media with non-trivial spin. Thus in hyperbolic-like elastic anisotropic materials, the spin-related strong coupling strength between circularly polarized elastic point load and these high DOS modes will realize the spin-selected elastic wave routing.

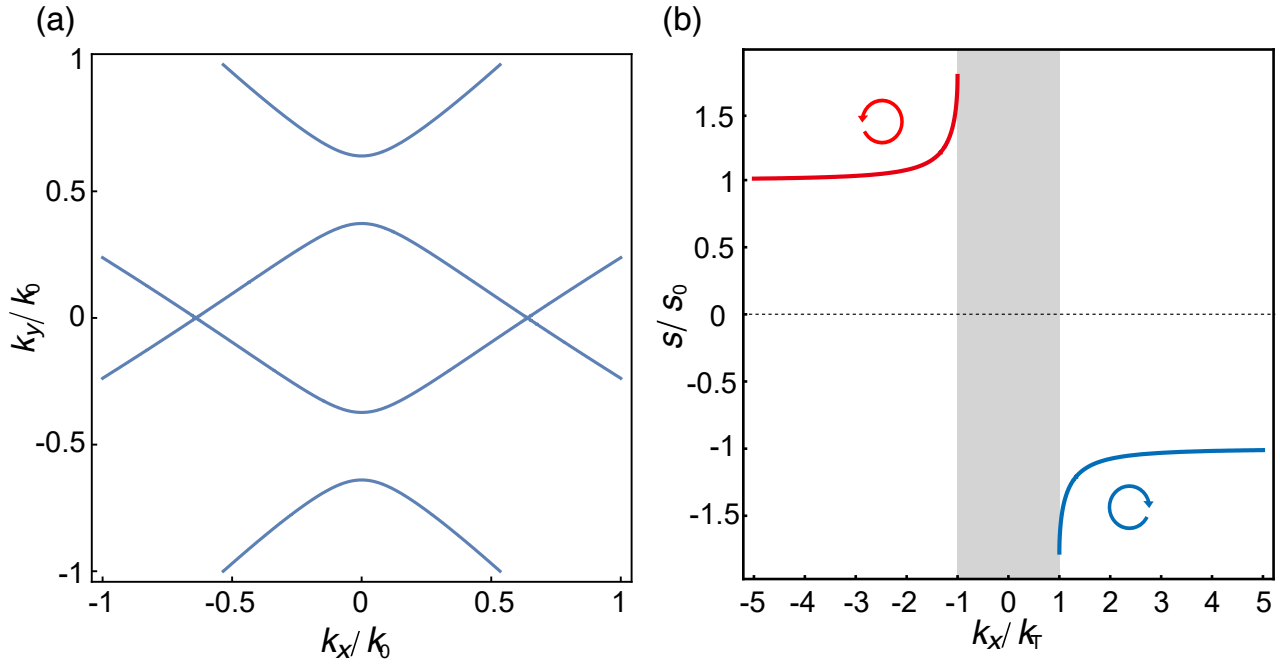

Fig. S5. Non-trivial spin Hall Effect (SHE) of elastic wave in bulk can be achieve in anisotropic media interfaced with isotropic media. (a) The equifrequency relationship of elastic wave in anisotropic media, which has the similar characteristic of hyperbolic relationship. (b) The spin angular momentum density s for evanescent wave in isotropic media side. In the gray area, the spin angular momentum density is degenerated and can not induce obvious coupling with high DOS modes in hyperbolic-like elastic media. But outside the gray area, the evanescent wave form will carry non-trivial spin and meanwhile induce strong spin-selected couplings.

If a circularly polarized point load is placed in isotropic side, in near-field proximity to the interface of the anisotropic elastic media with hyperbolic-like dispersion, shown in Fig.(4) of the main text, the wave emission will be efficiently coupled to the high local density of states (LDOS) modes. By calculating the spin angular momentum density of evanescent wave in isotropic material side based on Eq. 17, shown in Fig. S5(b), the induced evanescent wave possesses strong spin-momentum locked phenomena: different momentum directions with opposite spins. Thus when the circularly polarized point load excites the evanescent wave with non-trivial spin, and then they will highly couple with the corresponding high LDOS modes and excite one wave radiation propagating along a critical angle in hyperbolic-like elastic media. Similar with the spin-controlled results on boundary of isotropic media, the elastic spin $\boldsymbol{s}$ is responsible for unidirectional bulk elastic wave transport in anisotropic media, which can be regarded as elastic spin Hall effect (SHE). Elastic SHE can serve as a highly efficient approach to achieve the tunable confined elastic energy and information transport with selected directions. The anisotropic materials discussed here is mainly based on the elastic metamaterials, which can realize the arbitrary elastic parameters by designing micro-structure.

C. Comparing with QSHE of light. Comparing with QSHE of optics (3), there are several unique properties in elastic wave spin: (i) For elastic wave, the solid can support longitudinal propagation wave form in bulk, the counterpart of which can not be found in optics since electromagnetic waves are transverse. Longitudinal component in elastic waves contributes to both the orbital and spin angular momentum. And more specially, the longitudinal components can mix with the transverse components in elastic waves. Therefore, although the optic wave spin density only contains the contributions from transverse wave, $\boldsymbol{s} = \boldsymbol{s}_T$, the total elastic wave spin will additionally include the terms from longitudinal wave and the hybrid spin from longitudinal-transverse mixing, $\boldsymbol{s} = \boldsymbol{s}_L + \boldsymbol{s}_T + \boldsymbol{s}_h$. (ii) For optics, the surface plasmon modes can only be supported on the interface of two media with some specific conditions, i.e, metal and vacuum. For elastic wave, the surface mode, Rayleigh wave, appears on the solid boundary with free boundary conditions. The outside space does not support elastic wave, so that is a perfect elastic insulator. The Rayleigh wave can only exist in the single solid side of the boundary. (iii) For light, transverse electric field (TE) and transverse magnetic field (TM), reflects the dual symmetry of electromagnetic waves. For the surface mode of light, it merely holds either TE or TM mode (3), so the non-trivial QSHE is based on the dual-symmetry broken on interface. But for elastic wave, only Rayleigh wave will be considered for analyzing the spin, with a vanishing hybrid spin from longitudinal-transverse mixing, but with a restricted dispersion between longitudinal and transverse wave components.

4. Experimental scheme for QSHE of elastic wave

In this section, we provide an experimental scheme to observe the QSHE of elastic wave. To excite elastic wave with non-trivial spin, we should realize the circularly polarized point load firstly, namely $\boldsymbol{F} = F_x\boldsymbol{e}_x + iF_y\boldsymbol{e}_y$. Here, we use four elastic point sources with different phases to induce effective excitation effects of circularly polarized point load. The similar experimental scheme can also be found in electromagnetic wave (15, 16). In practices, the circularly polarized elastic point load can be realized by piezoelectric ceramics or laser beam array with different excitation phases. Here, we take piezoelectric ceramics scheme as example, shown in Fig. S6. Their phase patterns can be realized by introducing delays in the external AC driving circuits (for laser beam, it will be the optical lens system). With placing them into the cavities on the surface of aluminum shown in Fig. S6(b), one can excite the chiral elastic wave with non-trivial spin locally. It should be mentioned that the geometrical size of point source arrays would make influences about the final effective excitation effect. Actually, its size should be smaller than one wavelength of elastic wave to improve performances, so-called sub-wavelength regime, similar to the electromagnetic case (15, 16). One can reduce the size of sources or make experiments in lower frequency. It is easy to reduce the size for laser beam through the focusing function of optical lens.

To show the validity of this approach, we simulate the elastic field on aluminum excited by finite size source arrays in Fig. S6. From the numerical simulations for real cases, we can see that surface elastic wave will propagate along opposite directions for different phase patterns, which reflects the spin-momentum locking of elastic waves with opposite spins.

5. Simulation details

All numerical results are obtained by commercial finite element analysis software (COMSOL). The materials used in the simulations of Fig. 4(a,b) of the main text are aluminum, which has mass density $\rho = 2700kg/m^3$, Young's modulus $E = 70GPa$, and Poisson's ratio $\nu = 0.33$.

In Fig. 4(a) of the main text, the simulation area is the square block with side length $40cm$. Two chiral point loads are placed on the center of solid with a distance $1cm$ from each other. All boundaries are all set as low-reflecting boundary. To realize different circular-polarized point load, we set $F_x = 1/\sqrt{2}N$, and $F_y = \pm i/\sqrt{2}N$ to excite the corresponding waves with different spin: + for spin up, - for spin down. The exciting frequency is $f = 100kHz$.

In Fig. 4(b) of the main text, the simulation area is the rectangle block with width $100cm$ and height $40cm$. The point load is placed on the edge of solid with free boundary condition. Other boundaries are all set as low-reflecting boundary. The exciting frequency is $f = 100kHz$.

In Fig. 4(c) of the main text, the simulation area is the square block with side length $100cm$. The top block is anisotropic material and the bottom block is isotropic material. A circular-polarized point load is placed inside the isotropic solid and a short distance ($\approx 4cm$) from the interface between anisotropic material and isotropic material. The stiffness tensor used for the

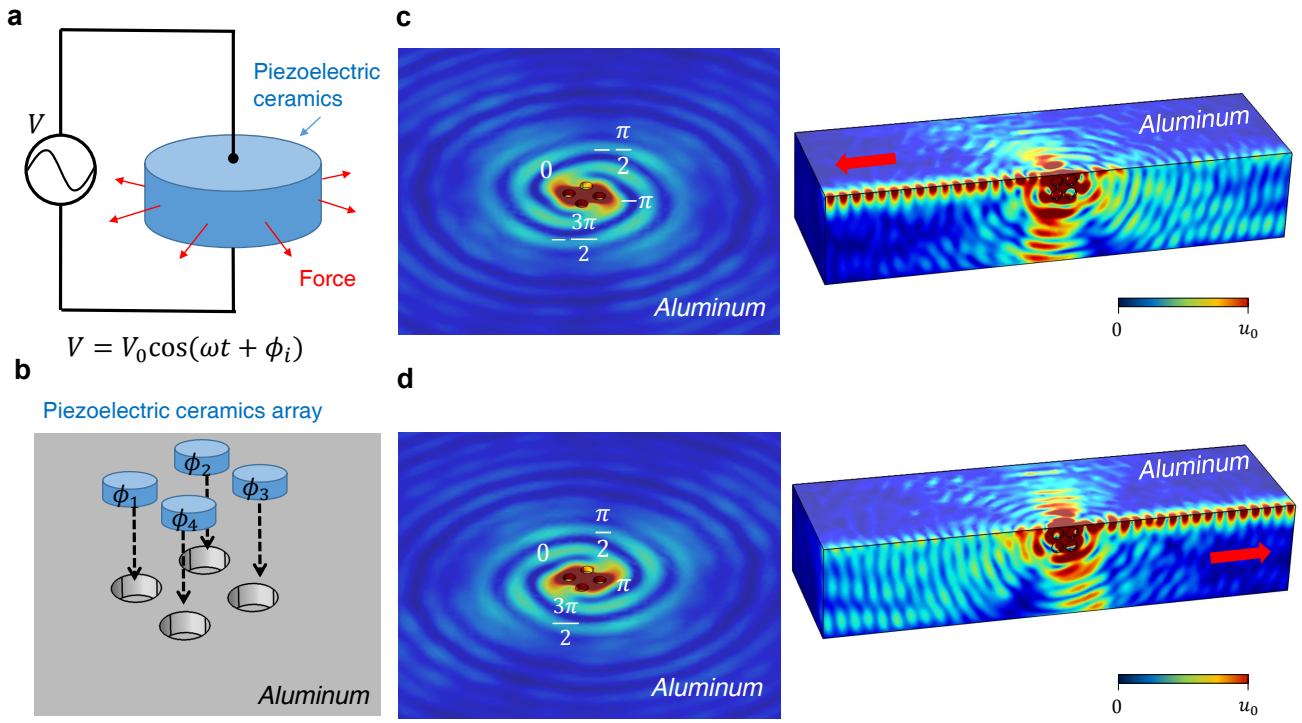

Fig. S6. Experimental scheme for QSHE of elastic wave. (a) Piezoelectric ceramics is driven by AC voltages with frequency ω and phase ϕ_i. (b) Four piezoelectric ceramics with different excitation phases are placed into four cavities on the surface of aluminum. The ϕ_1, ϕ_2, ϕ_3 and ϕ_4 are their excitation phases. This scheme will induce effective circularly polarized point load which would carry non-trivial spin density. (c) The amplitude of elastic field excited by these four piezoelectric ceramics. Their excitation phases are labeled with white digitals in plot: $\phi_1 = 0, \phi_2 = -\frac{\pi}{2}, \phi_3 = -\pi$ and $\phi_4 = -\frac{3\pi}{2}$. After placed this array into the boundary of aluminum block, it will excite uni-directional surface elastic wave. (d) $\phi_1 = 0, \phi_2 = \frac{\pi}{2}, \phi_3 = \pi$ and $\phi_4 = \frac{3\pi}{2}$. The uni-directional excitation of boundary mode can be realized by using different phase patterns, which reflects spin-momentum locking relationship (QSHE of elastic wave). The similar experimental schemes havs also been found in electromagnetic wave (15, 16).

anisotropic material is:

$$\boldsymbol{C}_{aniso,eff} = C_0 \begin{pmatrix} 0.17 & 0.33 & 0.33 & 0 & 0 & 0 \\ 0.33 & 0.5 & 0.33 & 0 & 0 & 0 \\ 0.33 & 0.33 & 0.67 & 0 & 0 & 0 \\ 0 & 0 & 0 & 0.17 & 0 & 0 \\ 0 & 0 & 0 & 0 & 0.17 & 0 \\ 0 & 0 & 0 & 0 & 0 & 0.17 \end{pmatrix}, \quad [18]$$

where $C_0 = 5.75GPa$, $\rho = 2.7g/cm^3$. For the isotropic material, it is:

$$\boldsymbol{C}_{iso,eff} = C_0 \begin{pmatrix} 0.67 & 0.33 & 0.33 & 0 & 0 & 0 \\ 0.33 & 0.67 & 0.33 & 0 & 0 & 0 \\ 0.33 & 0.33 & 0.67 & 0 & 0 & 0 \\ 0 & 0 & 0 & 0.17 & 0 & 0 \\ 0 & 0 & 0 & 0 & 0.17 & 0 \\ 0 & 0 & 0 & 0 & 0 & 0.17 \end{pmatrix}. \quad [19]$$

The exciting frequency of sources is set as $f = 5kHz$.

References

1. Auld BA (1973) *Acoustic fields and waves in solids.* (Wiley).
2. Belinfante FJ (1940) On the current and the density of the electric charge, the energy, the linear momentum and the angular momentum of arbitrary fields. *Physica* 7(5):449–474.
3. Bliokh KY, Smirnova D, Nori F (2015) Quantum spin hall effect of light. *Science* 348(6242):1448–51.
4. Bliokh KY, Bekshaev AY, Nori F (2014) Extraordinary momentum and spin in evanescent waves. *Nat. Commun.* 5(3):3300.
5. Berry MV (2009) Optical currents. *J Opt. A Pure Appl. Op* 11(9):094001.
6. Bekshaev A, Bliokh K, Soskin M (2010) Internal flows and energy circulation in light beams. *J Optics* 13(5):994–1001.
7. Kane CL, Mele EJ (2005) Quantum spin hall effect in graphene. *Phys. Rev. Lett.* 95(22):226801.
8. Kane CL, Mele EJ (2005) Z2 topological order and the quantum spin hall effect. *Phys. Rev. Lett.* 95(14):146802.
9. Moore JE (2010) The birth of topological insulators. *Nature* 464(7286):194–8.
10. Qi XL, Zhang SC (2010) The quantum spin hall effect and topological insulators. *Physics Today* 63(1):33–38.
11. Qi XL, Zhang SC (2011) Topological insulators and superconductors. *Reviews of Modern Physics* 83(4):1057.
12. Hasan MZ, Kane CL (2010) Colloquium: topological insulators. *Reviews of Modern Physics* 82(4):3045.
13. Jackiw R, Rebbi C (1976) Solitons with fermion number 1/2. *Physical Review D* 13(12):3398.
14. Schnyder AP, Ryu S, Furusaki A, Ludwig AW (2008) Classification of topological insulators and superconductors in three spatial dimensions. *Physical Review B* 78(19):195125.
15. Kapitanova PV, et al. (2014) Photonic spin hall effect in hyperbolic metamaterials for polarization-controlled routing of subwavelength modes. *Nat. Commun.* 5(2):3226.
16. Guo Z, et al. (2017) Photonic spin hall effect in waveguides composed of two types of single-negative metamaterials. *Sci. Rep.* 7.